Studies of Efficiency of the LHCb Muon Detector Using Cosmic Rays

Public Note

Issue: 1
Revision: 0

Reference: LHCb-PUB-2009-017
Created: October 15, 2009
Last modified: October 15, 2009

Prepared by: Giulia Manca[a], Liliana Mou[a], Biagio Saitta[a]
[a]University and I.N.F.N. Cagliari, Italy

LHCb-PUB-2009-017
15/10/2009

Abstract

We study the efficiency of the muon detector using the cosmic ray events collected in the summer and autumn 2008. We find that the efficiencies in all stations are consistent with 100% for cosmic tracks coming from the LHCb interaction point, in a large time window. We calculate the efficiencies also per station and region and per station and quadrant, finding consistent results.

Contents

1 Introduction

The installation of the LHCb muon detector in the cavern has been completed in early 2008, with the exception of the first station (M1), which has been added only recently. It has been included in several "global commissioning runs", where it was successfully operated together with the other sub-detectors as a whole. In most cases we collected cosmic rays events, selected by a combination of muon and calorimeter triggers. In absence of proton beam, these data are crucial to commission the detector and check the performances of its single components. In particular for the muon system, muons from cosmic ray events are extremely useful, as they are similar to the muons from interactions events, apart from the angular distribution.

We have studied cosmic ray events coming from different periods of data taking, and used the events to measure the efficiency of the muon system. In this document we present the results of these studies, and compare them with the results from preliminary tests performed on the individual chambers in similar conditions [2]. The efficiencies are estimated in a large time window and as such can be considered as an upper limit on the efficiencies of the detector in beam conditions. More details on these studies are given in an internal LHCb note on the same subject [1].

2 Overview of the LHCb Muon System

The muon system [2, 3, 4, 5], shown in Figure 1, is composed of five stations (M1-M5) of rectangular shape, placed along the beam axis. The full system comprises 1380 chambers and covers a total area of 435 m^2. The inner and outer angular acceptances of the muon system are 20 (16) mrad and 306 (258) mrad in the bending (non-bending) plane respectively.

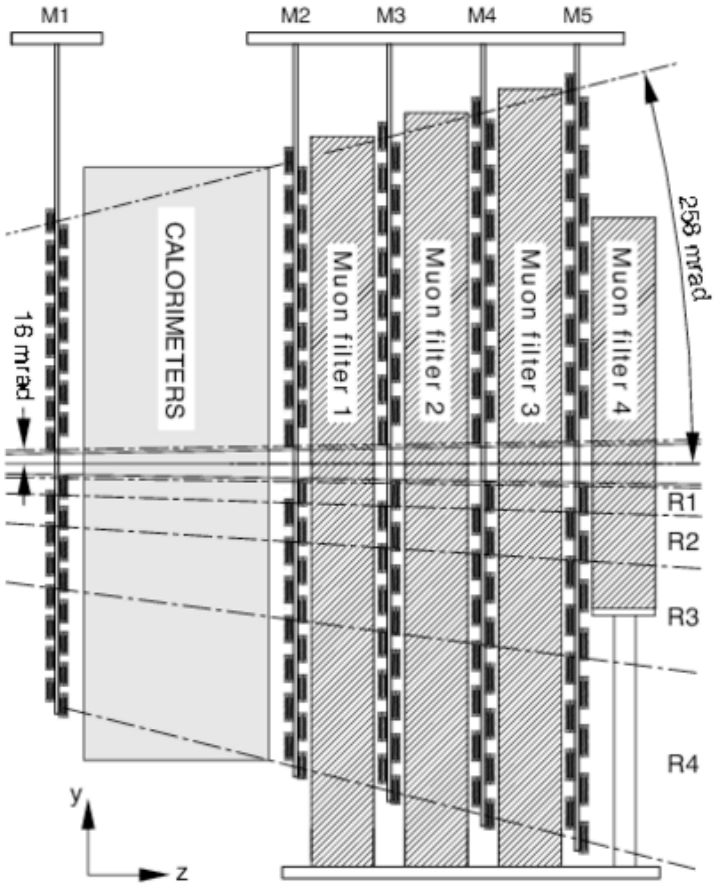

Figure 1 Side view of the muon system.

Stations M2 to M5 are placed downstream the calorimeters and are interleaved with iron absorbers 80 cm thick to select penetrating muons. The minimum momentum of a muon to cross the five stations is approximately 6 GeV/c. Station M1 is placed in front of the calorimeters in order to improve the p_{T} measurement in the trigger. The geometry of the five stations is projective, meaning that all their transverse dimensions scale with the distance from the interaction point. The detectors provide space point measurements of the tracks, sending binary information to the trigger processor and to the DAQ. The information is obtained by partitioning the detector into rectangular *logical pads* whose dimensions define the x, y resolution. Stations M1 to M3 have a high spatial resolution along the x coordinate (bending plane). Stations M4 and M5 have a limited spatial resolution, their main purpose being the identification of penetrating particles. The layout of the muon stations is shown in Figure 2. Each Muon Station is divided into four regions, R1 to R4 with increasing distance from the beam axis. The linear dimensions of the regions R1, R2, R3, R4, and their segmentations scale in the ratio 1:2:4:8. With this geometry, the particle flux and channel occupancy are expected to be roughly the same over the four regions of a given station. The (x, y) spatial resolution worsens far from the beam axis, where it is in any case limited by the increase of multiple scattering at large angles. The right part of Figure 2 shows schematically the partitioning of an example station into logical pads and the (x, y) granularity. Table 1 gives detailed information on the geometry of the muon stations.

3 Data

The studies include three sets of runs of cosmic events, close in time with each other and taken with the detector configured in similar way [a] in the Fall 2008. The High Voltage (HV) for these runs was 2.5

[a] The third set differs from the first two by three missing chambers and in the number of masked channels. These changes do not affect the final results in any significant way.

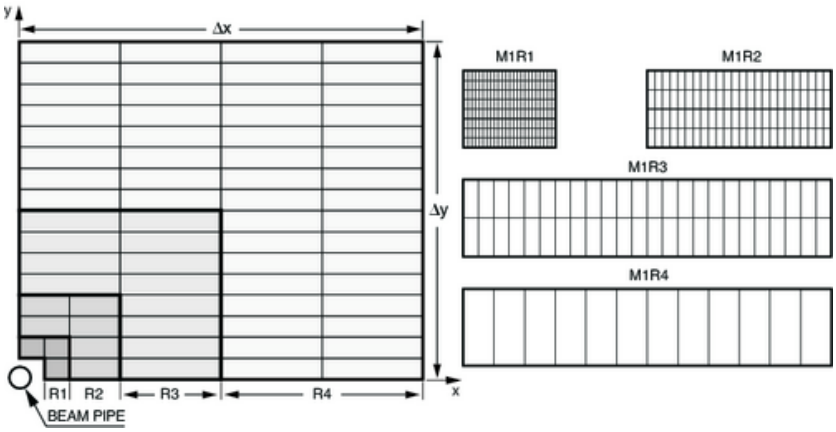

Figure 2 Left: front view of a quadrant of a muon station. Each rectangle represents one chamber. Each station contains 276 chambers. Right: division into logical pads of four chambers belonging to the four regions of station M1. In each region of stations M2-M3 (M4-M5) the number of pad columns per chamber is double (half) the number in the corresponding region of station M1, while the number of pad rows per chamber is the same (see Table 1).

Table 1 Basic information for the five stations M1–M5 and the four regions R1–R4. All dimensions in cm. z: distance of the stations from the interaction point; Δx and Δy: dimensions of a quadrant in each station (see Figure 2). Rows R1-R4: granularity of the different regions of the muon detector as seen by trigger and DAQ.

	M1	M2	M3	M4	M5
z	1210	1527	1647	1767	1887
Δx	384	480	518	556	594
Δy	320	400	432	464	495
R1	1×2.5	0.63×3.1	0.67×3.4	2.9×3.6	3.1×3.9
R2	2×5	1.25×6.3	1.35×6.8	5.8×7.3	6.2×7.7
R3	4×10	2.5×12.5	2.7×13.5	11.6×14.5	12.4×15.5
R4	8×20	5×25	5.4×27	23.1×29	24.8×30.9

kV, while the chamber thresholds were set between 1.3 and 1.5 times the nominal value of each channel [b], which has been defined after dedicated studies [6]. The events are time aligned in the hardware for muons coming from the interaction region. The time windows in which the events are accepted is expected to be of 25 ns in beam data. In order to allow the time alignment of the Muon System, for these runs the time window has been relaxed to accept events belonging to multiple bunch crossings around the central one. These events are defined Time Alignment Events (TAE) and the number of TAE indicates the number of bunch crossing accepted around the central one. In all the periods considered the gas mixture was Ar/CO_2 (40:55). The runs we used are summarised in Table 2. The plots shown in the following include all events from the three sets of runs (a total of 1406415 events), unless otherwise specified. The first station of the muon detector, M1, had not yet been installed by the time the data were collected and it is not included in the analysis.

Table 2 Information on the data used for this analysis.

RUN NUMBER	TRIGGER	# EVENTS	TAE	TIME WINDOW
33878-33893	calo(*)	530932	± 3	175 ns
34064-34120	calo or muon(**)	451499	± 3	175 ns
35664-35671	calo	425668	± 2	125 ns

(*) The trigger rate was 10 Hz.
(**) The events triggered only by the muon system were removed for the efficiency calculation. This results in 1684 events removed.

[b] This results in thresholds of about 5-7 fC on anode-readout chambers and 10-14 fC on the cathode ones.

3.1 Data Quality Checks

We have applied few preliminary selections in order to enhance the purity of the data. The occupancy of the muon chambers for the data analysed before any selection is applied is shown in Figure 3 for the stations M2 to M5 and the regions R1 to R4.

- In order to avoid constructing fake tracks due to random combinations of hits, we have removed the noisiest channels in the run by calculating the average pad occupancy per station and region (based on the plots in Figure 3). The channels which have a number of entries ten times higher than the average are removed. At this point the average is recalculated and the same procedure repeated until there is no channel which exceeds the limit. This results in the exclusion of 373 channels. The plot of the occupancy with these channels removed is shown in Figure 4.

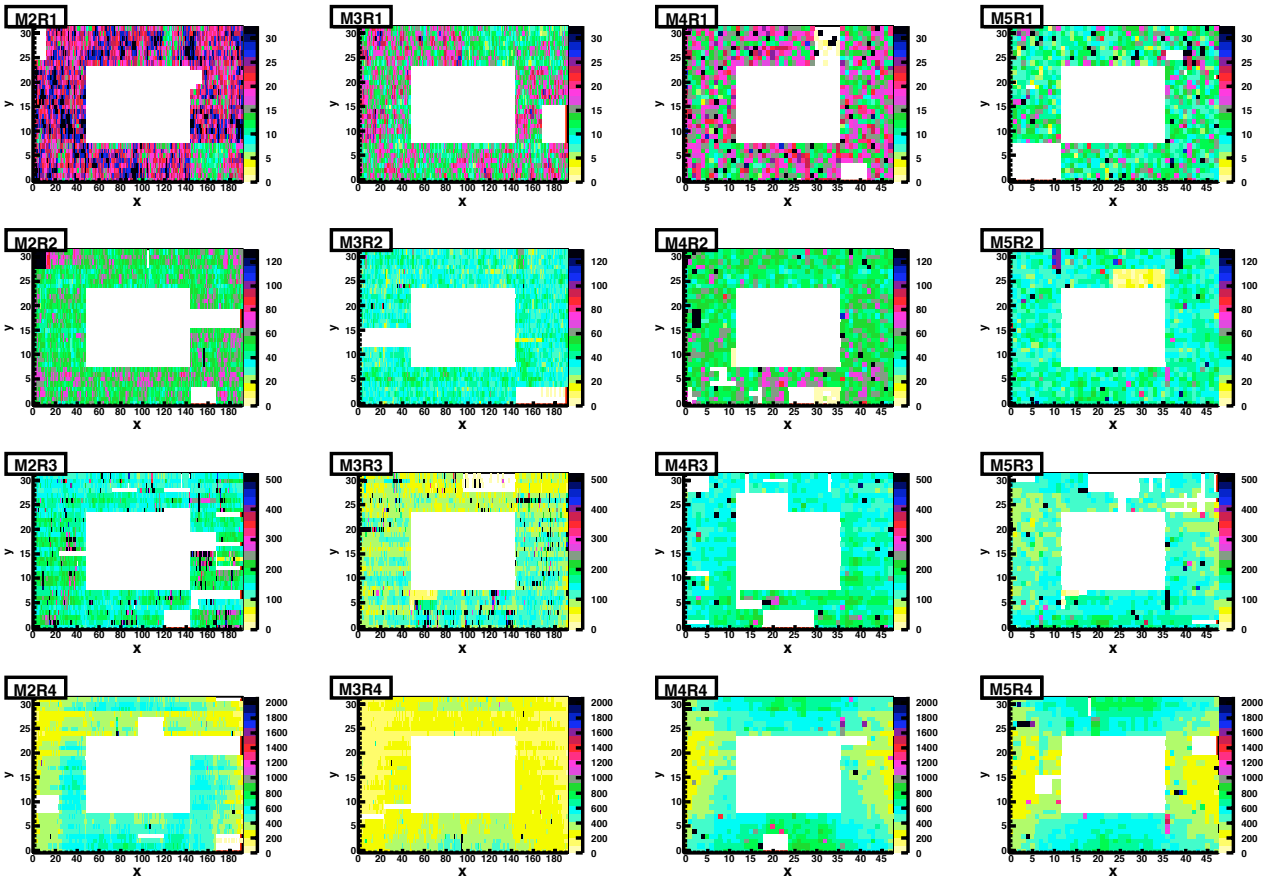

Figure 3 Logical pads occupancy for all the data described in the text for the stations M2 to M5 (left to right) and regions R1 to R4 (top to bottom), before any selection is applied to the data. For the plot of each region Ri the empty rectangle in the middle corresponds to the smaller region R(i-1); in the case of R1 it corresponds to the beam pipe. The other empty areas correspond to areas with masked or dead channels. The units of x and y are indicative of the x and y position of the hit, chosen such that each bi-dimensional bin corresponds to a logical pad.

- Some channels are dead or have been masked (corresponding to the empty regions in Figure 4). These channels account for about 5% of the total, and have been removed from the calculation of the efficiency. The effect of this removal is discussed in the following sections.
- In order to reduce the noise, events with total number of hits higher than 50 are removed from the analysis. These correspond to 5298 events. The average number of hits in the different stations after this removal is shown in Figure 5. The average number of hits is higher in M2 and M3, which are also the stations with the higher noise.

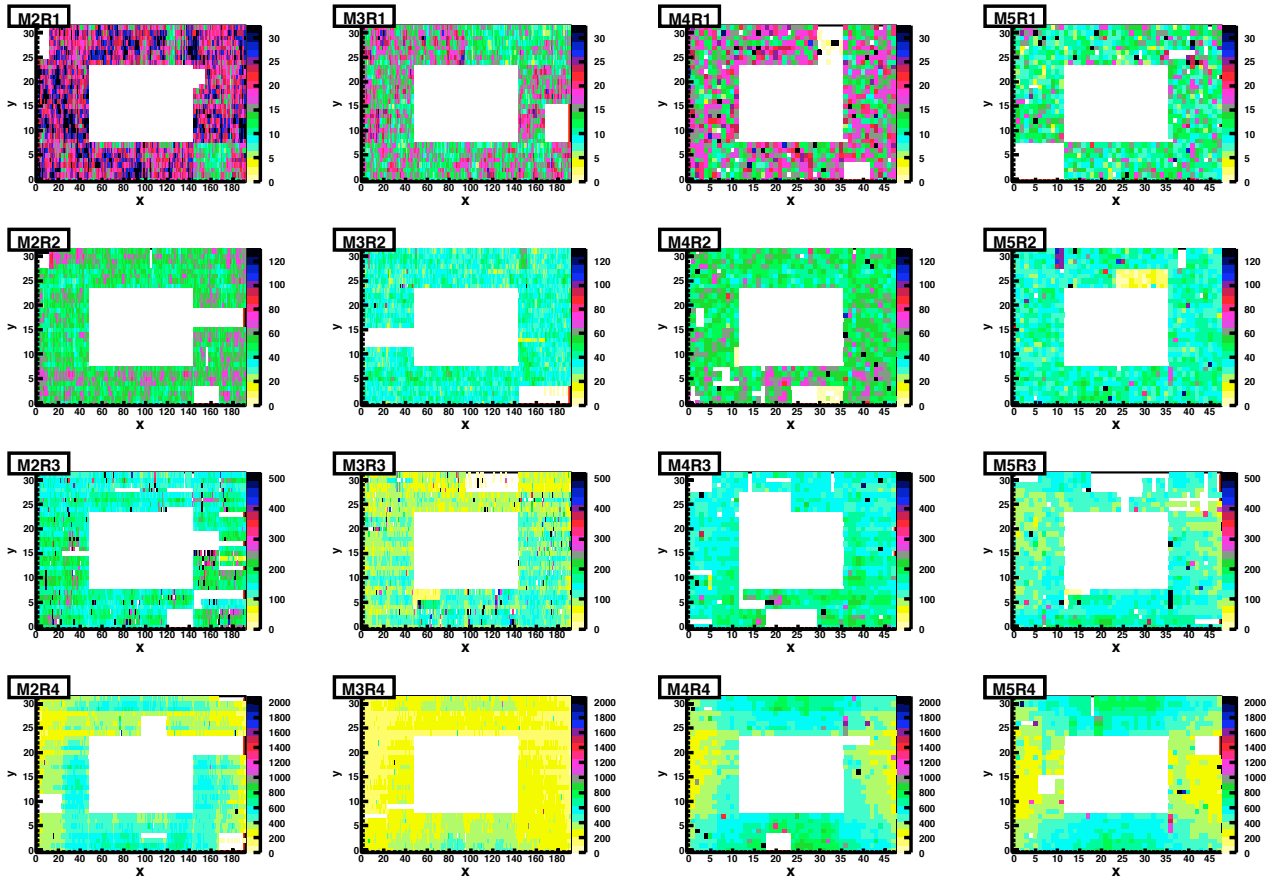

Figure 4 Logical pads occupancy for all the data described in the text for the stations M2 to M5 (left to right) and regions R1 to R4 (top to bottom), after the removal of the noisiest channels according to the procedure described in the text. For the plot of each region Ri the empty rectangle in the middle corresponds to the smaller region R(i-1); in the case of R1 it corresponds to the beam pipe. The other empty areas correspond to areas with masked or dead channels. The units of x and y are indicative of the x and y position of the hit, chosen such that each bi-dimensional bin corresponds to a logical pad.

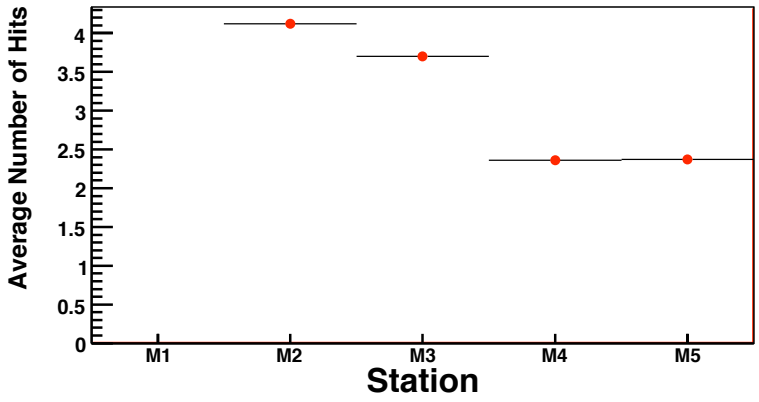

Figure 5 Average number of hits per station per event for the data described in the text.

4 Track Reconstruction

In each event we look for combinations of hits in three or four stations which could come from a track. To find four-hits' tracks, we combine each hit in M2 with each hit in M5 and look for hits in M3 and M4 closest to the interpolation in that station. We perform a three-dimensional chi squared fit of the four hits, using as uncertainty on the hit the size of the pad (in both dimensions) in that station and region, divided by $\sqrt{12}$, plus a contribution of 2.4 cm that we estimated [8] due to multiple scattering (MS), in the approximation where all tracks have the minimum momentum. To reconstruct tracks with three hits, we repeat the procedure using track seeds from combinations of hits in M2 and M4 or M3 and M5, choosing the hit in the missing station M3 or M4 closer to the interpolation. This procedure could result in multiple tracks per event. All the tracks so found are then ordered per decreasing χ^2 and per number of hits, being the four hits track with smallest χ^2 the first. The probability $P(\chi^2)$ distribution for the best track in each event is shown in Figure 6. The non-uniform distribution could be due to the approximate inclusion of the effect of multiple scattering. We select only tracks with $P(\chi^2)$ >0.05. We find 178052 tracks with four hits and 186071 with three hits satisfying this requirement. In Figure 8 the slopes of the fit to the tracks in x and y are shown; the two peaks at negative and positive y indicate the cosmic tracks which are going respectively forward and backward w.r.t. the interaction point. In Figure 9 we show the residuals between the found hits and the extrapolation values in x and y for the best tracks in the event, for all stations together. The distribution is broader in y than x as we expect from the granularity of the muon detector. The occupancy of the four stations and regions for the best track in the event is shown in Figure 7. We have found that 99% of the reconstructed tracks have at least a hit in one of the calorimeter systems, within the distance of one cell size from the extrapolation point, convoluted with the extrapolation uncertainty.

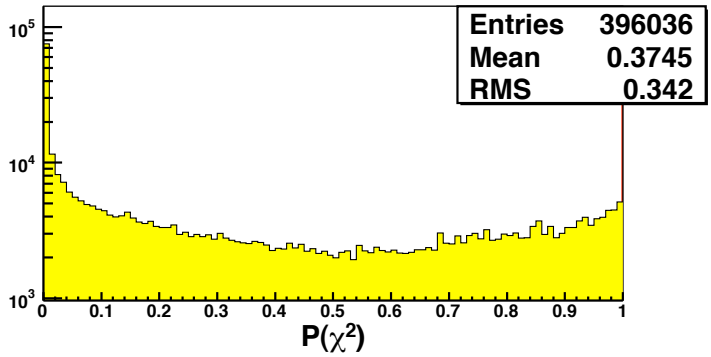

Figure 6 Distribution of P(χ^2) for the best track in each event. Only tracks with $P(\chi^2) > 0.05$ are kept in this analysis.

5 Efficiency Calculation

For the efficiency calculation we use the best track with three hits in each event, reconstructed as explained in the previous chapter. For each three-hits track, we look for hits in the missing station. If we find a hit, we use the parameters of the fit to extrapolate the expected position in x and y based on the z position of the hit. The extrapolated values are checked to be:

- *within the acceptance of the detector*, meaning we have required the extrapolated point to be at least 3σ (the uncertainty on the extrapolation) away from the borders of the station; when the efficiency is calculated per region and quadrant, the same requirement to the borders is not applied for statistical reasons;
- *not in a dead region of the detector*, where we have required the extrapolated value not to be in one of the emptys regions of the plots in Fig. 4, without including any uncertainties for the points on the borders.

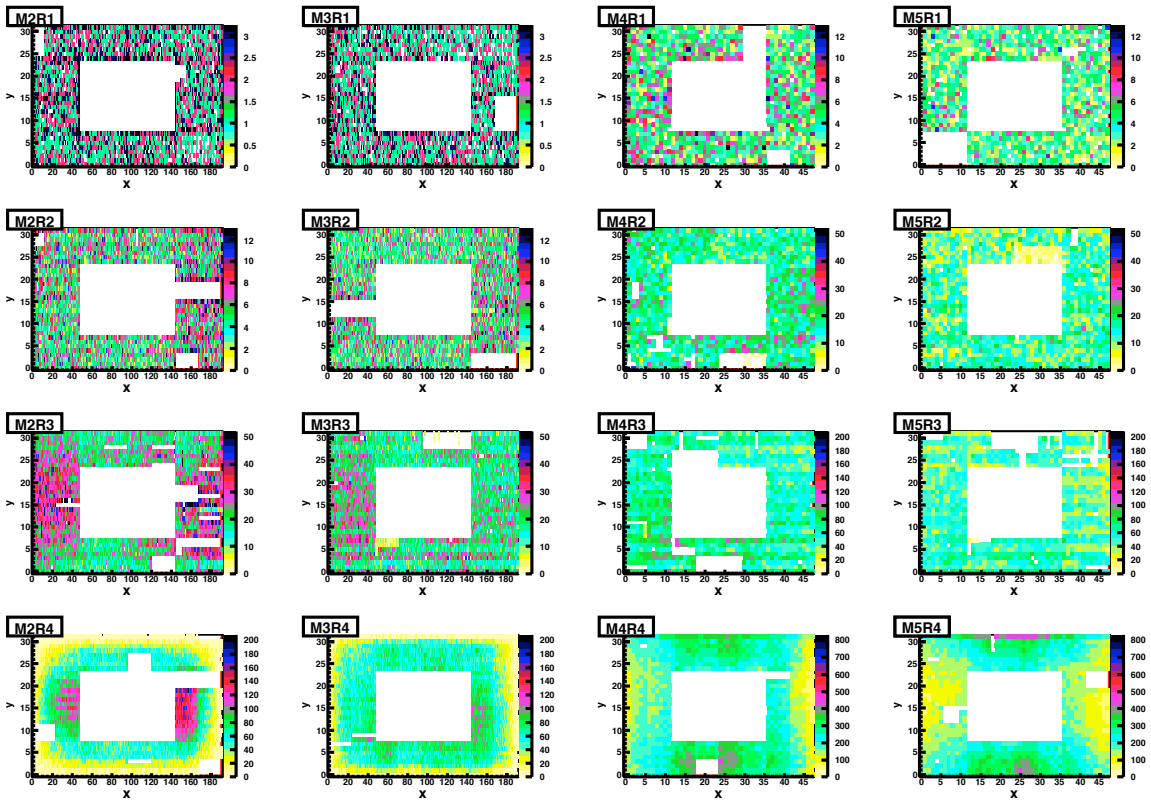

Figure 7 Logical pads occupancy for the best track in each event in the data, for the stations M2 to M5 (left to right) and regions R1 to R4 (top to bottom). For the plot of each region Ri the empty rectangle in the middle corresponds to the smaller region R(i-1); in the case of R1 it corresponds to the beam pipe. The other empty areas correspond to areas with masked or dead channels. The units of x and y are indicative of the x and y position of the hit, chosen such that each bi-dimensional bin corresponds to a logical pad.

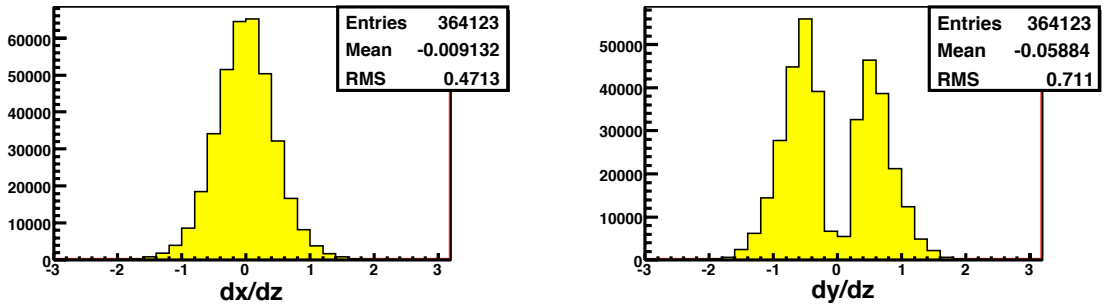

Figure 8 Distribution of the slopes in x (*left*) and y (*right*) for the best track for each event.

If they satisfy these requirements, the extrapolated x and y are compared with the x and y of the hit found. We select the hit with the smallest two-dimensional distance from the extrapolated value. If this distance is less than the size of half a pad in that station and region, convoluted with the uncertainty on the extrapolation (corresponding to 3σ), then we say we found a hit. If there is no hit in the missing station, we use the z position of the middle of the station for the extrapolation. If the extrapolated values are within acceptance (and at least 3σ away from the borders as explained before), these events are also counted in the denominator of the efficiency, which is defined as:

$$\epsilon = \frac{M}{N},$$

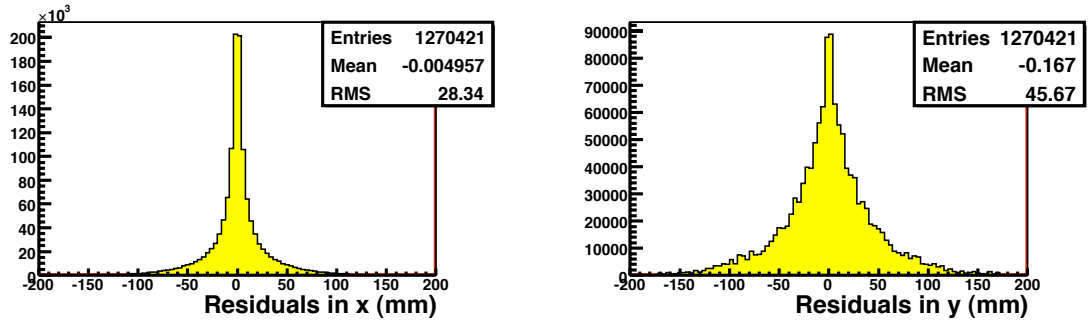

Figure 9 Distribution of the residuals in x (*left*) and y (*right*) for the hits of the best track for each event, for all stations.

where:

N is the number of events with a three hits' track, for which we found a hit in the missing station. The extrapolated x and y value of this hit, estimated using the true z of the hit and the parameters of the fit, are within the acceptance of the chambers.

M represents the events for which the true x and y of the hit are close to the extrapolated x and y values, as explained in the text.

The effect of the background has been estimated using a run of noise taken with the chambers in similar conditions and found to be negligible for this analysis. The total efficiencies for each station are shown in Table 3. We refer to the efficiency calculated in this way as "raw". The procedure is repeated for each region and quadrant within each station, and the results reported in Table 4 and Table 5. The values of the raw efficiencies are roughly uniform in the four quadrants of the same station for all stations apart for M2, where the Q1 is less efficient than the others. From Fig 3 we observe Q1 has a large number of dead areas, which could affect the raw efficiency. The raw efficiencies are different in the different regions, being lower in the inner region R1 (where the statistics is also lower) and growing in the outer regions. This could be due to several reasons:

- the larger pad size in R3 and R4, which translates in more relaxed criteria of search of the hit;
- the smaller size of the chambers in the inner regions, which also means more gaps and thus less acceptance;
- the treatment of the borders in the acceptance check could have a larger effect in the inner regions than in the outer.

Table 3 Total raw efficiency for the four stations of the LCHb muon detector. The uncertainties are statistical.

	M2	M3	M4	M5
ϵ	(82.8$\pm$ 0.1)%	(85.7$\pm$ 0.1)%	(89.4$\pm$ 0.1)%	(88.5$\pm$ 0.1)%

The raw efficiencies are of the order of 85% on average. Not removing the dead channels results in a decrease of 5% of the efficiencies.
The major source of inefficiency is the non-projectivity of the tracks. In fact the muon detector is built to be completely hermetic for tracks which are coming from the interaction point by a suitable overlap of the chambers in the stations. The same is not true for cosmic tracks, which come from several different angles, preferably vertical [7]. These tracks could then hit uninstrumented areas of the detector, mimicking an inefficiency. In order to isolate this effect we introduced the projectivity angle θ_i^p, defined for each station Mi as the three-dimensional angle the track forms with the line

Table 4 Total raw efficiency for the four stations and regions of the LCHb muon detector. The uncertainties are statistical.

Region	M2	M3	M4	M5
R1	(72.6± 1.0)%	(67.4± 0.8)%	(79.2± 0.9)%	(84.0± 1.0)%
R2	(73.8± 0.4)%	(73.1± 0.4)%	(83.8± 0.4)%	(85.3± 0.4)%
R3	(78.6± 0.2)%	(80.4± 0.2)%	(86.5± 0.2)%	(86.2± 0.2)%
R4	(86.5± 0.1)%	(90.1± 0.1)%	(90.9± 0.1)%	(89.4± 0.1)%

Table 5 Total raw efficiency for the four stations and quadrants of the LCHb muon detector. The uncertainties are statistical.

Quadrant	M2	M3	M4	M5
Q1	(80.1± 0.2)%	(84.4± 0.2)%	(89.6± 0.2)%	(88.4± 0.2)%
Q2	(83.4± 0.2)%	(86.7± 0.1)%	(90.2± 0.1)%	(89.4± 0.1)%
Q3	(83.3± 0.2)%	(85.1± 0.2)%	(88.4± 0.1)%	(87.3± 0.2)%
Q4	(83.7± 0.2)%	(86.3± 0.2)%	(89.5± 0.1)%	(89.0± 0.2)%

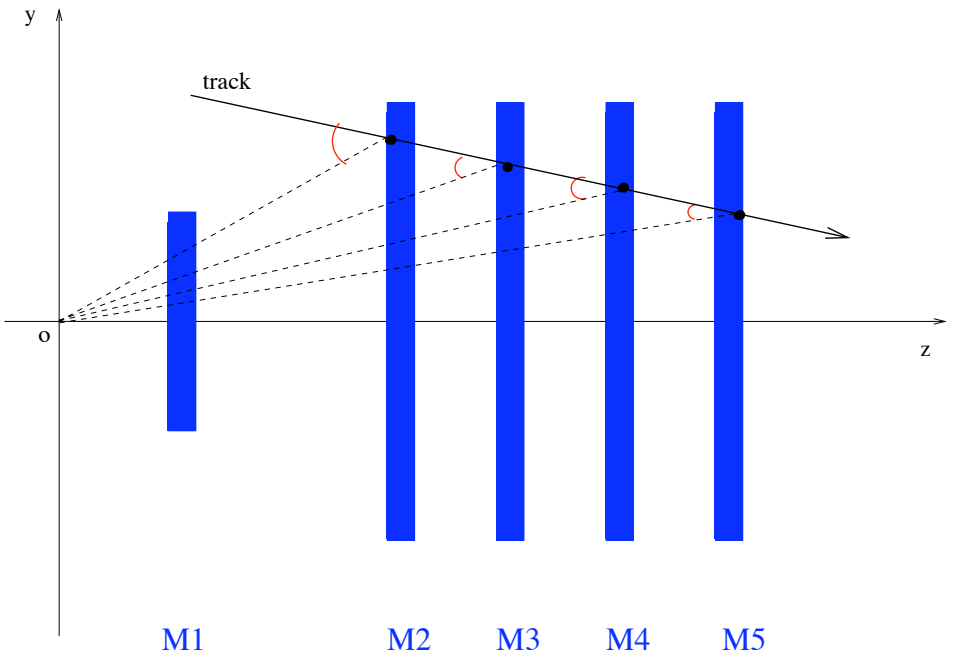

Figure 10 Indicative two dimensional representation of the LHCb muon detector on the yz plane, with the stations indicated in green. The two-dimensional projectivity angle θ_i^p is indicated in red for the i-th station. The drawing is not to scale.

connecting the hit with the interaction point (as illustrated in Fig. 10 for the bidimensional case). In a situation of perfect projectivity this angle is zero, and it grows as further away the track is from being projective. In Fig. 11 we show the distribution of θ_i^p for the best tracks with four hits in the event, for the four muon stations.

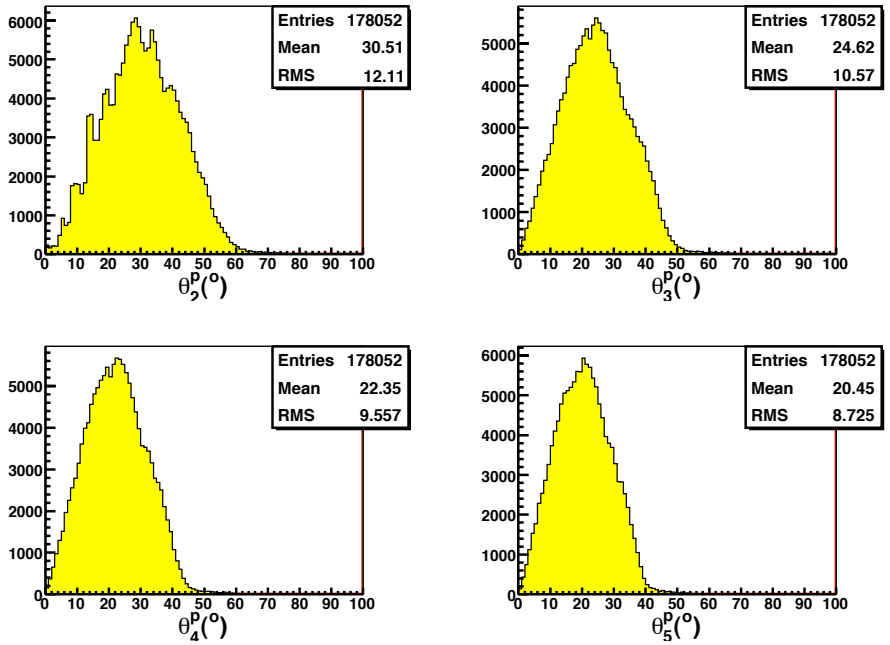

Figure 11 Distribution of the three-dimensional projectivity angle $\theta_i^p, i = 2-5$ for the four stations in tracks with four hits, for M2 (top left), M3 (top right), M4 (bottom left) and M5 (bottom right).

By analysing the dependence of the efficiency from the angle with a simple model, we found that it depends linearly on the tangent of θ_i^p, according to the formula

$$\epsilon = 1 - f \tan\theta^p,$$

where θ^p is the angle θ_i^p in the space, assuming normal incidence on the chambers, and f is a parameter which depends on the geometry of the detector.

We calculated the efficiency as a function of tanθ for the four stations, and for each station per region and per quadrant. The results are shown in Fig. 12 and Fig. 13 to Fig. 20. The efficiency is maximal for small angles for all stations, as we would expect for projective tracks. The trend is the same for all four stations. The raise for values of tanθ $\sim$ 0.5 are due to a geometrical effect. The efficiency distributions have been fitted between the values of $\tan\theta_i^p$ of 0 and 0.35 and the constraint $\epsilon <= 1.0$. The extrapolation at $\tan\theta = 0$ of the function would correspond to the value of the efficiency in a situation of perfect projectivity. The results are summarised in Table 6, 7 and 8 for the four different stations, regions and quadrants. The central values of the efficiencies are all consistent with 100%. The

Table 6 Efficiency corrected for the non-projectivity of the track for the four stations of the LCHb muon detector. The first uncertainty is statistical, the second systematic.

	M2	M3	M4	M5
ϵ	(98.0$\pm$ 0.4 $\pm$ 1.5)%	$(100.0^{+0.0+0.0}_{-0.2-1.8})\%$	$(100.0^{+0.0+0.0}_{-0.2-0.1})\%$	(99.2$\pm$ 0.3 $\pm$0.8)%

efficiencies are uniform in all quadrants of the same station, and are affected by the lack of statistics in some of the regions. The first uncertainties are the statistical uncertainties coming from the uncertainty on the fit, as shown in Fig. 13 to 16. In order to estimate the systematic contribution, we have calculated the efficiencies using a fit over the values of tanθ_i^p between 0 and 0.7. and taken the differences between the two central values as systematic uncertainty. This is the second uncertainty shown in Tables 6, 7 and 8. The inefficiency due to the presence of channels which are dead or have been masked has already been taken into account. Inefficiencies due to noise are expected to be small.

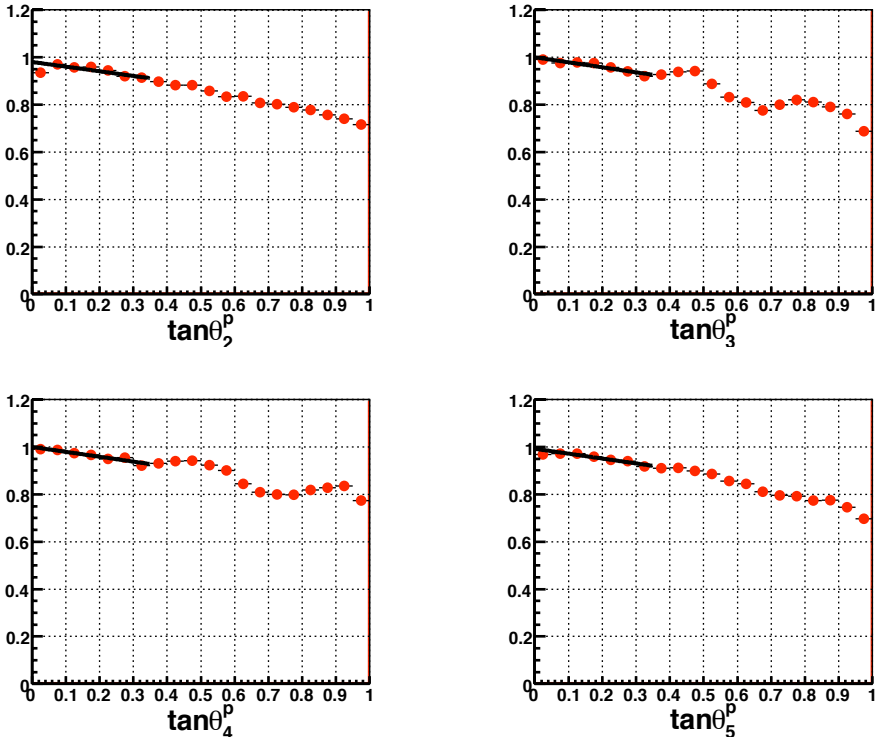

Figure 12 Efficiency of the four muon station M2 (top left), M3 (top right), M4 (bottom left) and M5 (bottom right) as a function of the tangent of the projectivity angle θ_i^p described in the text. The fit with a straight line is also shown, between the values of $\tan\theta$ of 0 and 0.35.

Table 7 Efficiency corrected for the non-projectivity of the track, per station and region. The first uncertainty is statistical, the second systematic.

Region	M2	M3	M4	M5
R1	$(100.0^{+0.0+0.0}_{-8.3-5.7})\%$	$(88.4^{+11.6+11.6}_{-12.6-22.8})\%$	$(100.0^{+0.0+0.0}_{-14.8-8.1})\%$	$(100.0^{+0.0+0.0}_{-9.3-6.9})\%$
R2	$(96.0\pm 4.6 \pm 0.3)\%$	$(98.3^{+1.7+1.7}_{-3.4-7.2})\%$	$(100.0^{+0.0+0.0}_{-3.3-2.5})\%$	$(100.0^{+0.0+0.0}_{-0.5-4.7})\%$
R3	$(94.8\pm1.4\pm2.3)\%$	$(98.1\pm1.3\pm 2.3)\%$	$(99.0^{+1.0+1.0}_{-1.1-1.6})\%$	$(98.6\pm1.0\pm0.6)\%$
R4	$(98.7\pm0.4\pm0.9)\%$	$(100.0^{+0.0+0.0}_{-0.2-1.4})\%$	$(100.0^{+0.0+0.0}_{-0.1-0.2})\%$	$(99.0\pm0.3 \pm 1.5)\%$

Table 8 Efficiency corrected for the non-projectivity of the track, per station and quadrant. The first uncertainty is statistical, the second systematic.

Quadrant	M2	M3	M4	M5
Q1	$(98.4\pm0.9\pm0.6)\%$	$(100.0^{+0.0+0.0}_{-0.2-1.4})\%$	$(100.0^{+0.0+0.0}_{-0.1-0.8})\%$	$(100.0^{+0.0+0.0}_{-0.5-0.1})\%$
Q2	$(93.7\pm0.9\pm2.9)\%$	$(100.0^{+0.0+0.0}_{-0.2-1.6})\%$	$(100.0^{+0.0+0.0}_{-0.1-0.7})\%$	$(99.9^{+0.1+0.1}_{-0.5-0.7})\%$
Q3	$(100.0^{+0.0+0.0}_{-0.2-1.1})\%$	$(99.8^{+0.2+0.2}_{-0.6-2.2})\%$	$(99.6\pm 0.5 \pm 0.3)\%$	$(98.3\pm0.6\pm1.3)\%$
Q4	$(100.0^{+0.0+0.0}_{-0.7-1.8})\%$	$(100.0^{+0.0+0.0}_{-0.4-2.1})\%$	$(100.0^{+0.0+0.0}_{-2.3-0.4})\%$	$(98.7\pm0.6 \pm 1.5)\%$

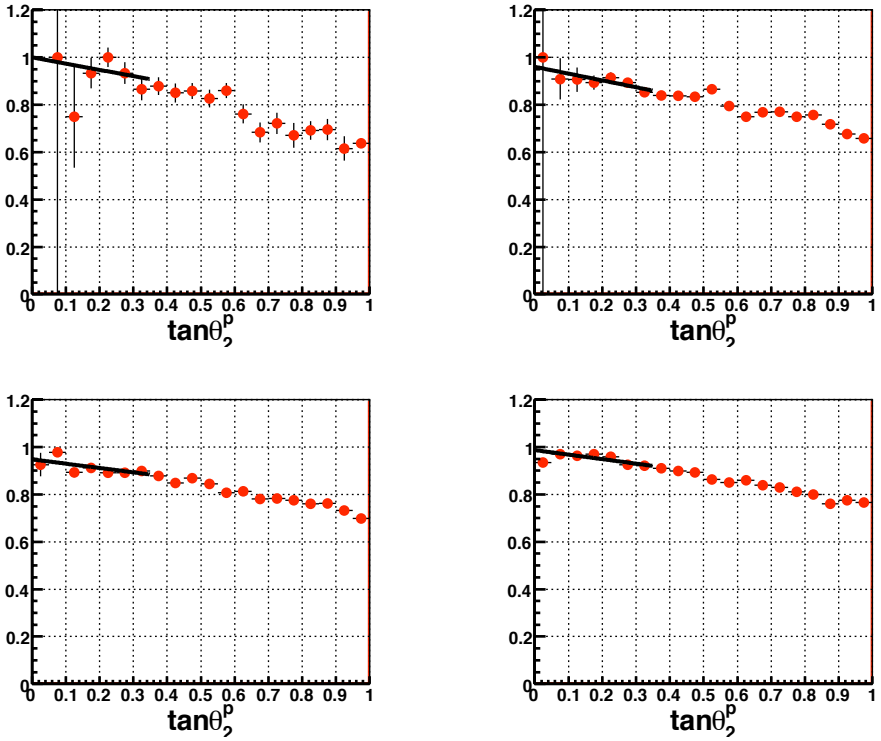

Figure 13 Efficiency of the four regions R1 (top left), R2 (top right), R3 (bottom left) and R4 (bottom right) of the station M2 as a function of the tangent of the projectivity angle θ_i^p described in the text. The fit with a straight line is also shown, between the values of $\tan\theta$ of 0 and 0.35.

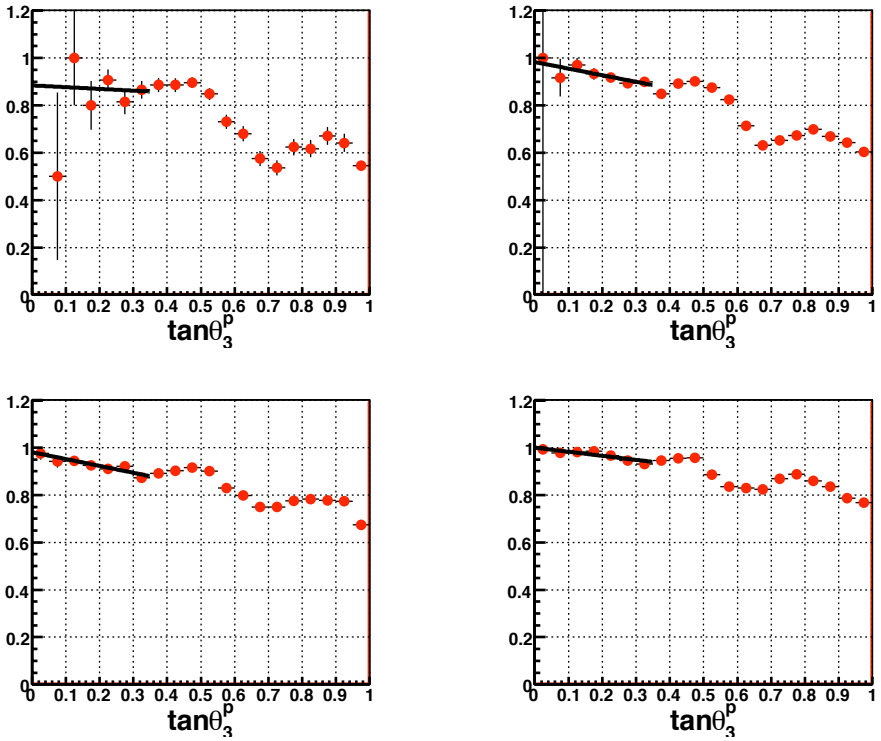

Figure 14 Efficiency of the four regions R1 (top left), R2 (top right), R3 (bottom left) and R4 (bottom right) of the station M3 as a function of the tangent of the projectivity angle θ_i^p described in the text. The fit with a straight line is also shown, between the values of $\tan\theta$ of 0 and 0.35.

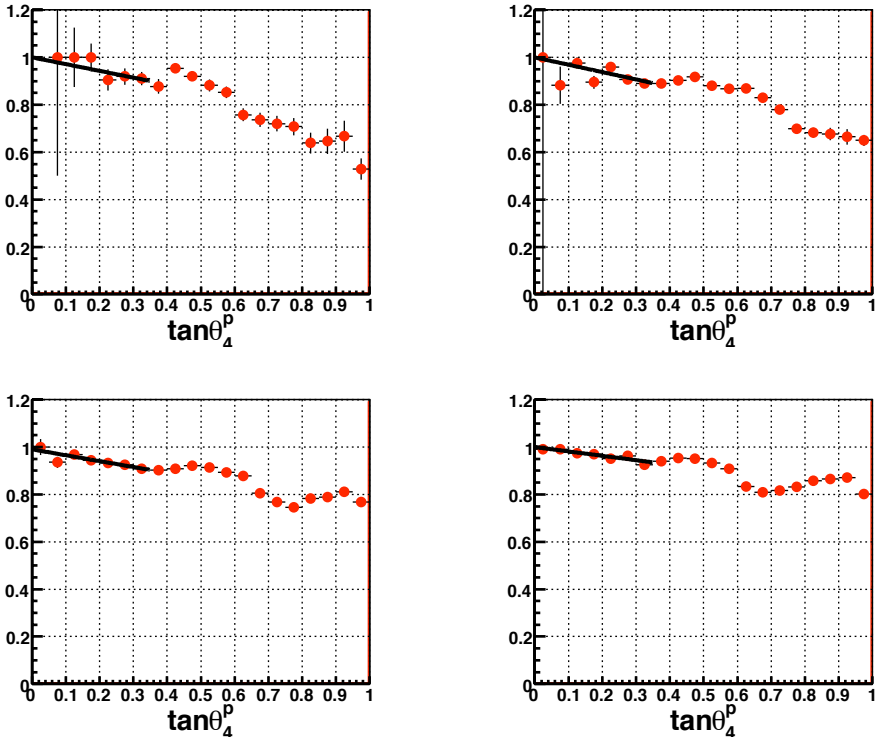

Figure 15 Efficiency of the four regions R1 (top left), R2 (top right), R3 (bottom left) and R4 (bottom right) of the station M4 as a function of the tangent of the projectivity angle θ_i^p described in the text. The fit with a straight line is also shown, between the values of $\tan\theta$ of 0 and 0.35.

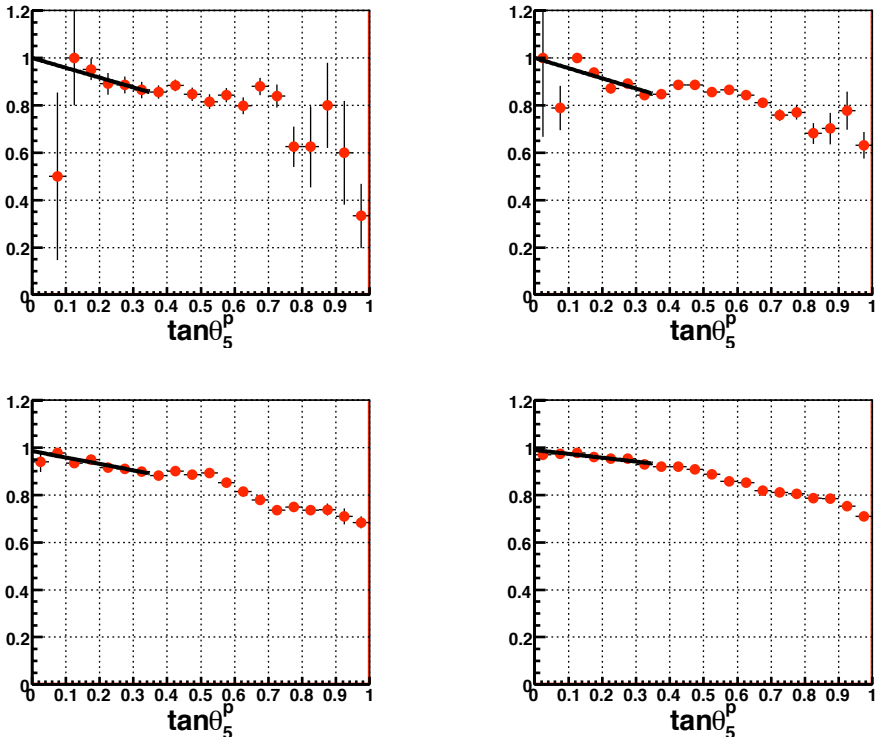

Figure 16 Efficiency of the four regions R1 (top left), R2 (top right), R3 (bottom left) and R4 (bottom right) of the station M5 as a function of the tangent of the projectivity angle θ_i^p described in the text. The fit with a straight line is also shown, between the values of $\tan\theta$ of 0 and 0.35.

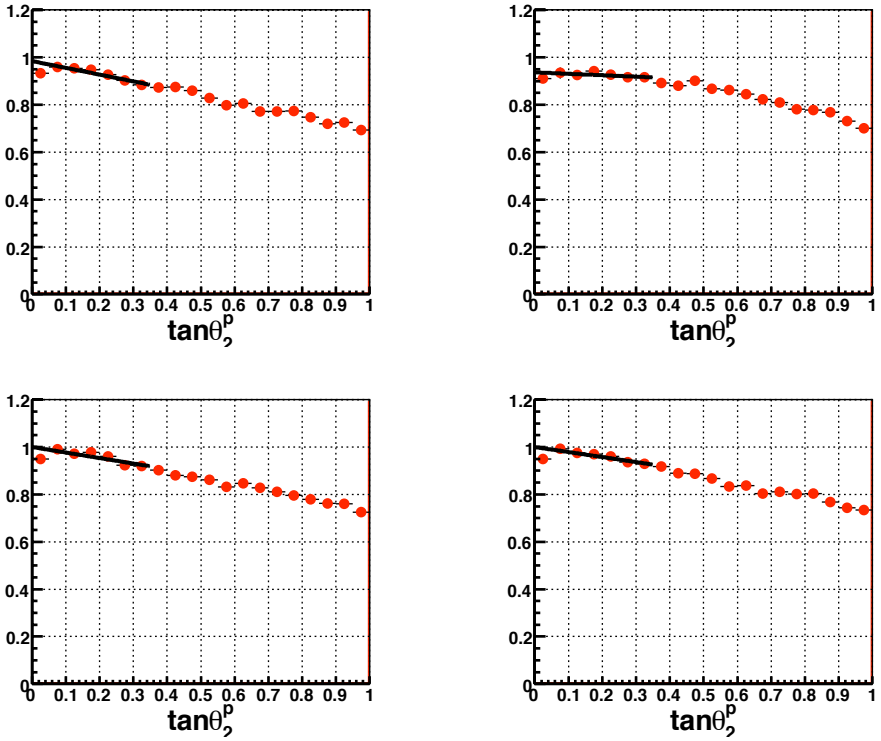

Figure 17 Efficiency of the four quadrants Q1 (top left), Q2 (top right), Q3 (bottom left) and Q4 (bottom right) of the station M2 as a function of the tangent of the projectivity angle θ_i^p described in the text. The fit with a straight line is also shown, between the values of $\tan\theta$ of 0 and 0.35.

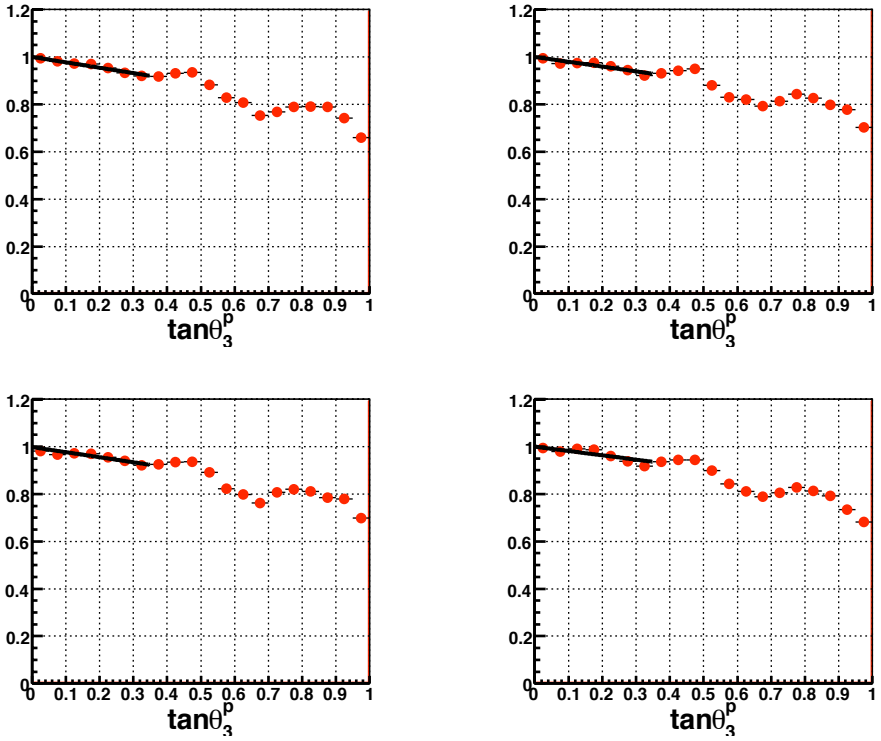

Figure 18 Efficiency of the four quadrants Q1 (top left), Q2 (top right), Q3 (bottom left) and Q4 (bottom right) of the station M3 as a function of the tangent of the projectivity angle θ_i^p described in the text. The fit with a straight line is also shown, between the values of $\tan\theta$ of 0 and 0.35.

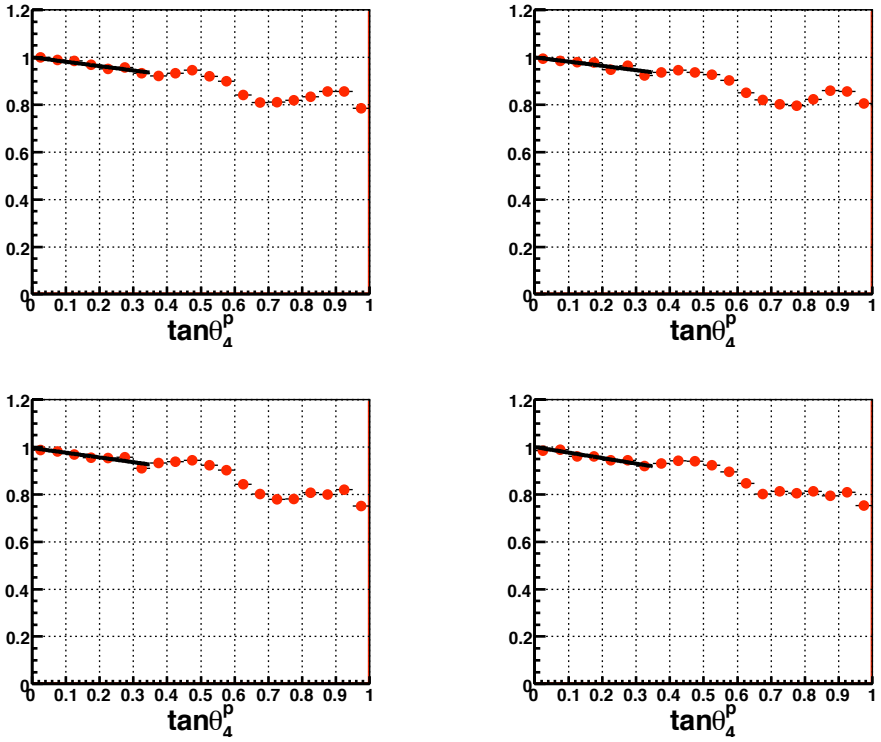

Figure 19 Efficiency of the four quadrants Q1 (top left), Q2 (top right), Q3 (bottom left) and Q4 (bottom right) of the station M4 as a function of the tangent of the projectivity angle θ_i^p described in the text. The fit with a straight line is also shown, between the values of $\tan\theta$ of 0 and 0.35.

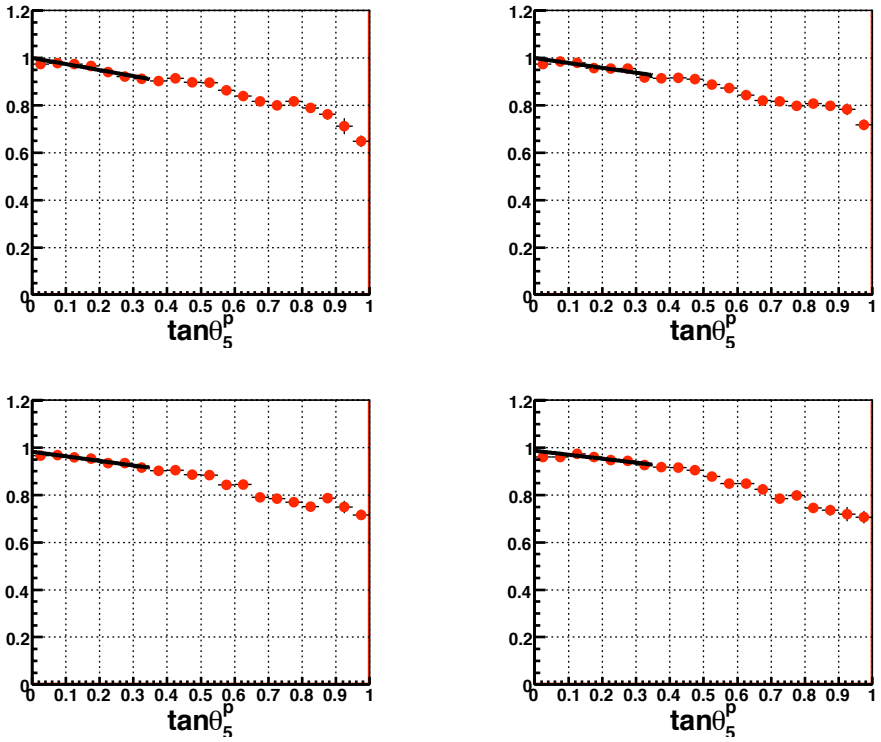

Figure 20 Efficiency of the four quadrants Q1 (top left), Q2 (top right), Q3 (bottom left) and Q4 (bottom right) of the station M5 as a function of the tangent of the projectivity angle θ_i^p described in the text. The fit with a straight line is also shown, between the values of $\tan\theta$ of 0 and 0.35.

6 Conclusions

We have studied the efficiencies of the LHCb muon detector using cosmic tracks. We have found that the main source of inefficiency is the non projectivity of the cosmic rays. To isolate this effect, we have selected the most projective tracks in the event and extrapolated the efficiency of the chambers in a situation of perfect projectivity. We found that the efficiency is consistent with 100% in all stations While the efficiency per station and quadrant is also consistent with 100%, the efficiency per station and region suffers from the lack of statistics in certain areas and as such should be revisited in the future when more data will become available. Preliminary tests had been performed on the chambers before the installation using cosmic rays and test beam data [2]. In those tests the efficiency of single chambers was measured, as a function of the High Voltage. Different gaps set-ups were used, at a fixed value of thresholds of 8 and 14 fC for the a cathode and anode readout respectively. The single chamber efficiency was found to be 96% and 98% for the four gaps configuration, at 2.5 kV, for cosmic ray events. The time window considered was 20 ns, close to the value which will be used with beam data. Considered the differences in data taking conditions, the previous results are compatible with our findings, although the statistics we have available does not allow us to measure the single chamber efficiency. We plan to update this work with more tests when new data will become available.

7 Acknowledgements

We would like to thank Giuseppe Martellotti, Giovanni Passaleva and Giacomo Graziani for useful discussions and comments on this work. We thank Giovanni Carboni for carefully reading this manuscript and giving useful comments on how to improve the results. We would also like to thank Walter Bonivento, Sandro Cadeddu, Caterina Deplano, Adriano Lai and Rolf Oldeman for closely following this analysis.

8 References

[1] G. Manca *et al.*, **LHCB Internal Note LHCb-INT-2009-026**.

[2] The LHCb Collaboration, The LHCb Detector at the LHC **Journal of Instrumentation (JINST), 3 S08005** (2008).

[3] LHCb Collaboration, *LHCb Muon System Technical Design Report*, CERN/LHCC 2001-010.

[4] LHCb Collaboration, *LHCb Addendum to the Muon System Technical Design Report*, CERN/LHCC 2003-002.

[5] LHCb Collaboration, *LHCb Second Addendum to the Muon System Technical Design Report*, CERN/LHCC 2005-012.

[6] A. Sarti *et al.*, **LHCB Public Note LHCb-2008-052**.

[7] D. Reyna, A simple parameterization of the cosmic-ray muon momentum spectra at the surface as a function of zenith angle, **arXiv:hep-ph/0604145**.

[8] C. Amsler *et al.*, **Physics Letters B**667, 1 (2008).